Supplementary Information

On the thermally oxidized CdS as a photoactive material

Anita Trenczek-Zajac
AGH University of Science and Technology, Faculty of Materials Science and Ceramics, al. A. Mickiewicza 30, 30-059 Krakow, Poland
anita.trenczek-zajac@agh.edu.pl

1. TEM analysis

TEM images were obtained using a JOEL-JEM1011 transmission electron microscope and presented in Fig.S1. CdS nanopowder is significantly agglomerated; however, small grains (2-12 nm) are pronounced.

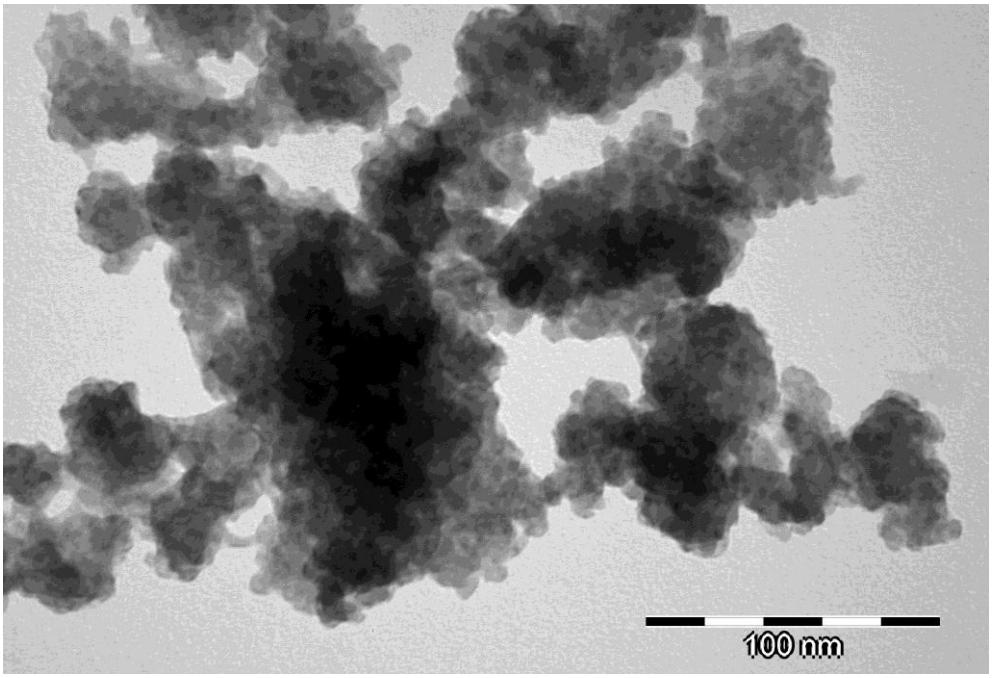

Figure S1. TEM image of CdS nanopowder.

The specific surface area (SSA) of CdS was determined from Brunauer-Emmett-Teller (BET) nitrogen adsorption isotherms obtained with the Nova 1200e (Quantachrome). SSA, defined as the total surface area per unit of mass, was used to calculate the nanoparticles'

diameter under the assumption that the samples exhibit nonporous, monodisperse and spherical morphology. In this case, SSA can be expressed by the formula (E1):

$$r_{avg} = \frac{3}{SSA \cdot \sum(x_i \cdot \rho_i)} \qquad \text{(E1)}$$

where *x* is the volume ratio of each phase, ρ denotes density, and *i* is the appropriate phase.

CdS nanopowder SSA = 145.4 $m^2 \cdot g^{-1}$, which correspond to BET – equivalent particle diameters equal to 8.5 nm. This result is highly consistent with that obtained from the analysis based on TEM images.

2. XRD analysis

The as-prepared CdS nanopowders and those annealed at 300^{o}C or below practically do not differ in terms of phase composition. As can be seen in Fig. S2a, only one broad peak is visible between 24 and 30^o, which may suggest that these samples consists of single phases crystallizing in the cubic structure of hawleyite (JCPDS-ICDD #01-075-0581). Similar conclusions concerning the XRD patterns of annealed CdS nanopowders were drawn by White et al.[1]. However, as observed by Trenczek-Zajac et al., an analysis of the 2θ range of 39-60^o (inset in Fig. S2a) reveals raised intensity between peaks at 44^o and 52^o corresponding to (220) and (311) reflections of the cubic phase, respectively[2]. This indicates the presence of the (103) reflection originating from the hexagonal phase of greenockite (JCPDS-ICDD #00-041-1049).

After annealing at 400^{o}C, pronounced temperature-induced changes in the crystal structure of the samples are observed (Fig. S2b). Instead of one broad peak, several new ones can be observed. Both hexagonal and cubic CdS phases are present, as evidenced by intense peaks at 25.0^o and 28.1^o, respectively; however, the hexagonal one is predominant. It can also be noticed that all peaks are much narrower when compared with those for 300^{o}C. This arises from the significant increase in the crystallite size of the annealed powder. Additionally, the following products of the partial oxidation process of CdS become visible, still as minority phases at this point: orthorhombic cadmium sulfate $CdSO_4$ (JCPDS-ICDD #01-086-1558) and monoclinic cadmium disulfate $Cd(S3O_7)$ (JCPDS-ICDD #01-078-1874). $Cd(S3O_7)$ was first found by Simonov et al., and is not observed very often[3]. However, similar structures of disulfates were prepared and identified by the group of Wickleder: $Re_2O_4Cl_2(S3O_7)$[4], $M[Au(S3O_7)_2]$ (M=Li, Na)[5], $Pd(S3O_7)$[6], and $Hg(S3O_7)$[4]. It was previously stated by

Zhensheng et al. that 400°C is the temperature at which cadmium sulfate(VI) $CdSO_4$ crystallizes when heating CdS in air[7]. Based on X-ray photoelectron spectroscopy (XPS), they also suggested that the partial transformation of CdS into $CdSO_4$ occurs at the surface of the sample. $Cd(S3O_7)$ was first found by Simonov et al., and is not observed very often[3]. However, similar structures of disulfates were prepared and identified by the group of Wickleder: $Re_2O_4Cl_2(S3O_7)$[4], $M[Au(S3O_7)_2]$ (M=Li, Na)[5], $Pd(S3O_7)$[6], and $Hg(S3O_7)$[4].

As can be seen in Fig. S2c, annealing at 500°C leads to the disappearance of cubic CdS, which is likely partially transformed into the more stable hexagonal form and partially oxidized into other phases. A comparison between the diffraction patterns obtained at 400°C and 500°C reveals further growth of crystallites as well as an increased contribution of the oxidized phases, i.e. $CdSO_4$ and $Cd(S3O_7)$. Moreover, there are some weak reflections that can be attributed to Cd_5S4O_6 (JCPDS-ICDD #00-045-1221), which can also be expressed as $2CdS{\cdot}2CdO{\cdot}CdSO_4$. Its presence in the Cd-S-O system was discovered by Fukatsu et al.[8].

The diffraction pattern for the CdS powder annealed at 600°C is again distinctly different from that recorded for the sample obtained at 500°C. Four major differences can be noticed in Fig. S2d: peak width decreases, the proportions between peak intensity change, new reflections appear, and the elevated background in the range between 23 and 33° lowers to the level of the baseline. All this suggests further growth of crystallites, the crystallization of some amorphous phase which was initially present in the precipitated CdS nanopowder, further reaction of sulfide with oxygen, and the formation of orthorhombic Cd_3SO_6 (JCPDS-ICDD #00-032-0140). $CdSO_4{\cdot}2CdO$ is one of the oxidized phases that can be found in the Cd-S-O system. Y. Wei et al. annealed CdS/ZnO core-shell nanofibers prepared with the use of the electrospinning technique and they found that Cd_3SO_6 forms after annealing at 600°C[9]. Some weak reflections in the studied samples remain unidentified and are marked with an asterisk.

Significant changes in diffraction patterns occurred yet again when the temperature was raised from 600°C to 700°C, as seen in Fig. S2e. Firstly, at this temperature hexagonal CdS transforms almost entirely into oxygen-containing phases and its reflections can barely be identified. Mohamed and El-Hagary also observed the disappearance of CdS above 700°C[10]. Secondly, all of the most intense reflections can be attributed to Cd_3SO_6, which is the majority phase after annealing at this temperature.

Above 700°C (Fig. S2f), changes in the X-ray pattern indicate further decay of CdS, $CdSO_4$, $Cd(S3O_7)$ and Cd_5S4O_6; the intensity of the reflections originating from these phases are extremely small. As in the case of the nanopowder oxidized at 600°C, Cd_3SO_6 is the

majority phase. However, a cadmium oxide CdO (JCPDS-ICDD #01-075-0591) peak appears at 800°C and is slightly more pronounced at 900°C. Literature sources concerning the presence of CdO in the process of CdS oxidation report its crystallization at 400°C[7,11] or above 620°C[10].

All described transformations are presented in Table T1.

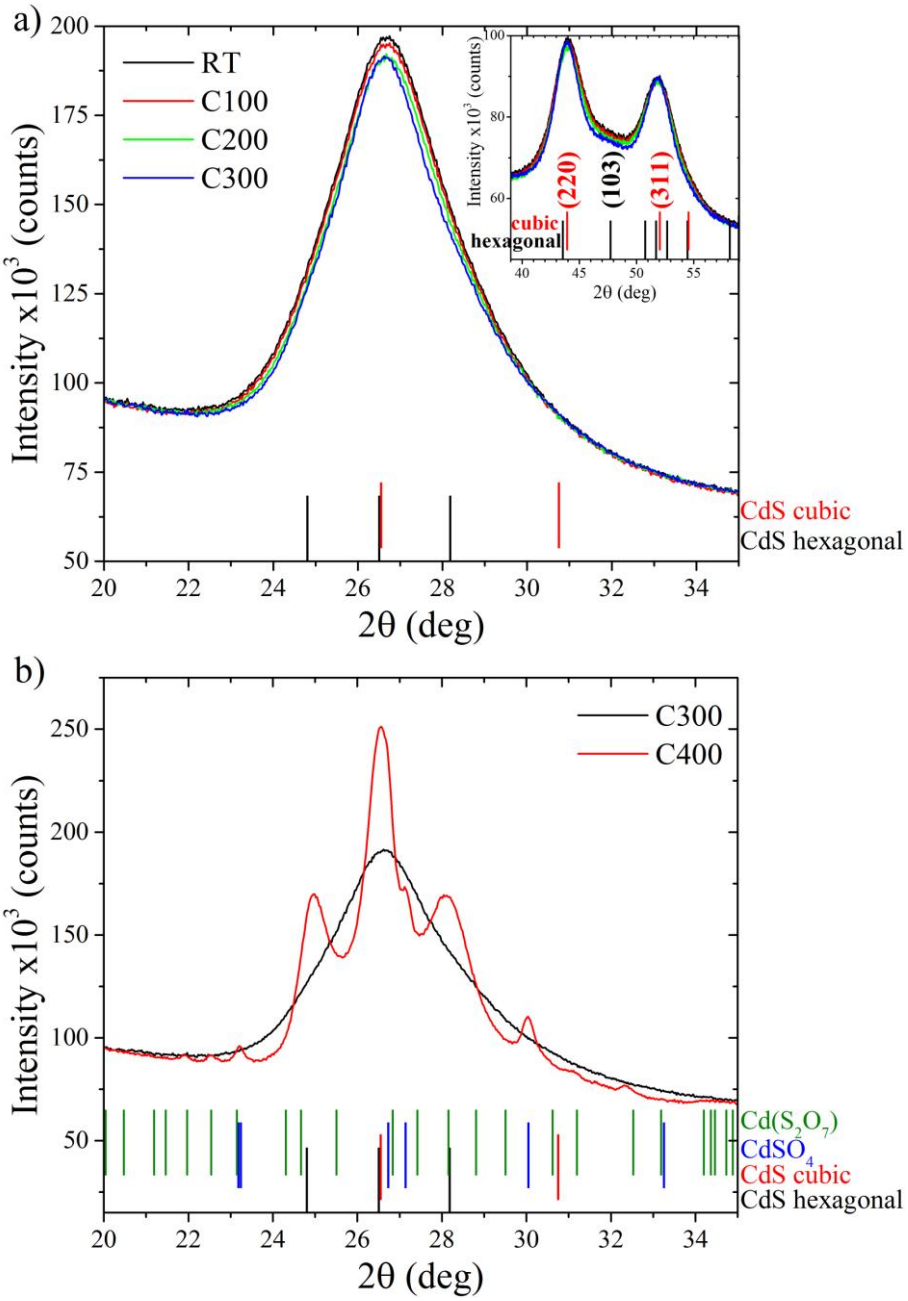

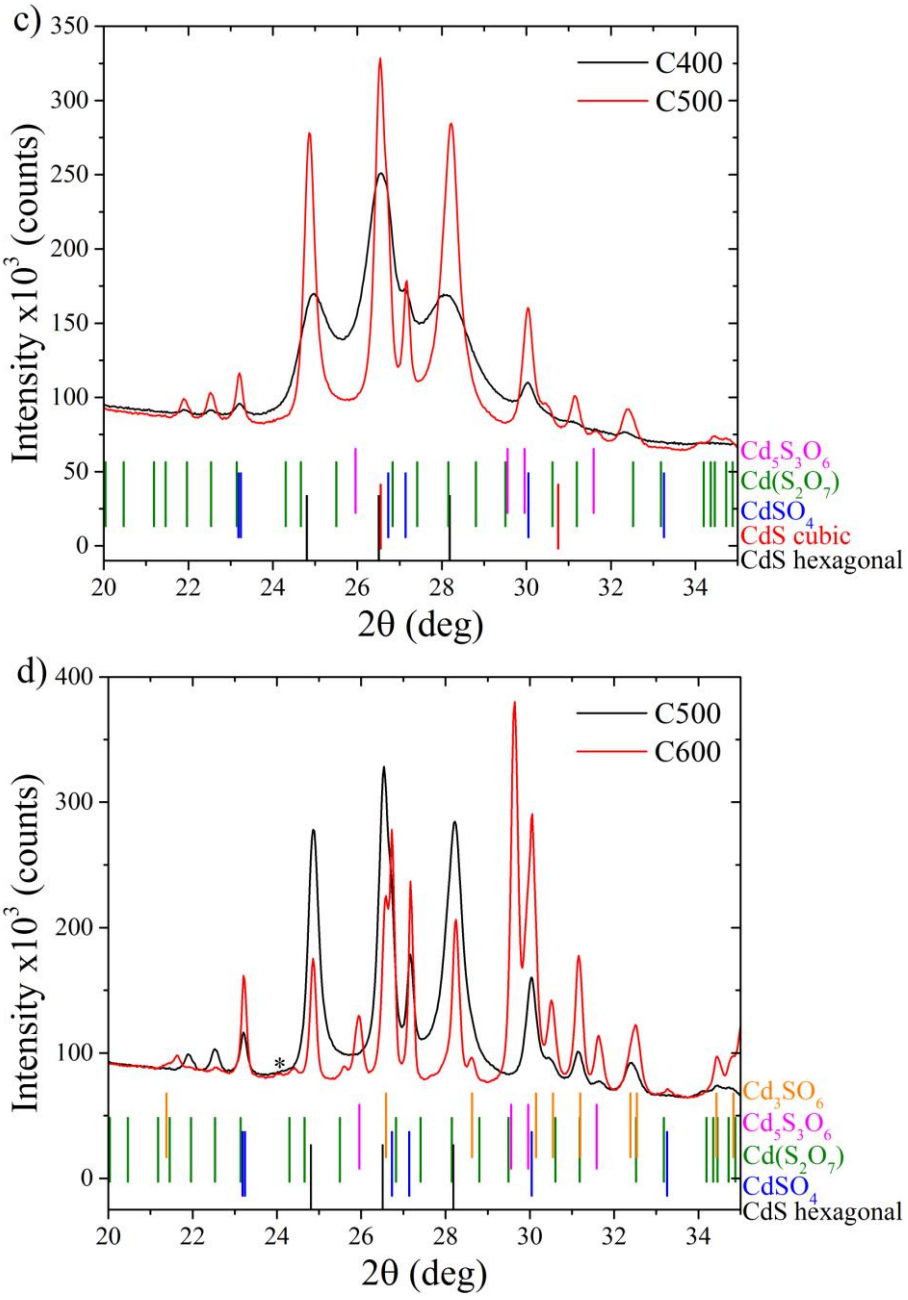
c)
Intensity x10^3 (counts)
2θ (deg)
C400
C500
$Cd_2S_3O_6$
$Cd(S_2O_7)$
$CdSO_4$
CdS cubic
CdS hexagonal
d)
Intensity x10^3 (counts)
2θ (deg)
C500
C600
Cd_3SO_6
$Cd_2S_3O_6$
$Cd(S_2O_7)$
$CdSO_4$
CdS hexagonal

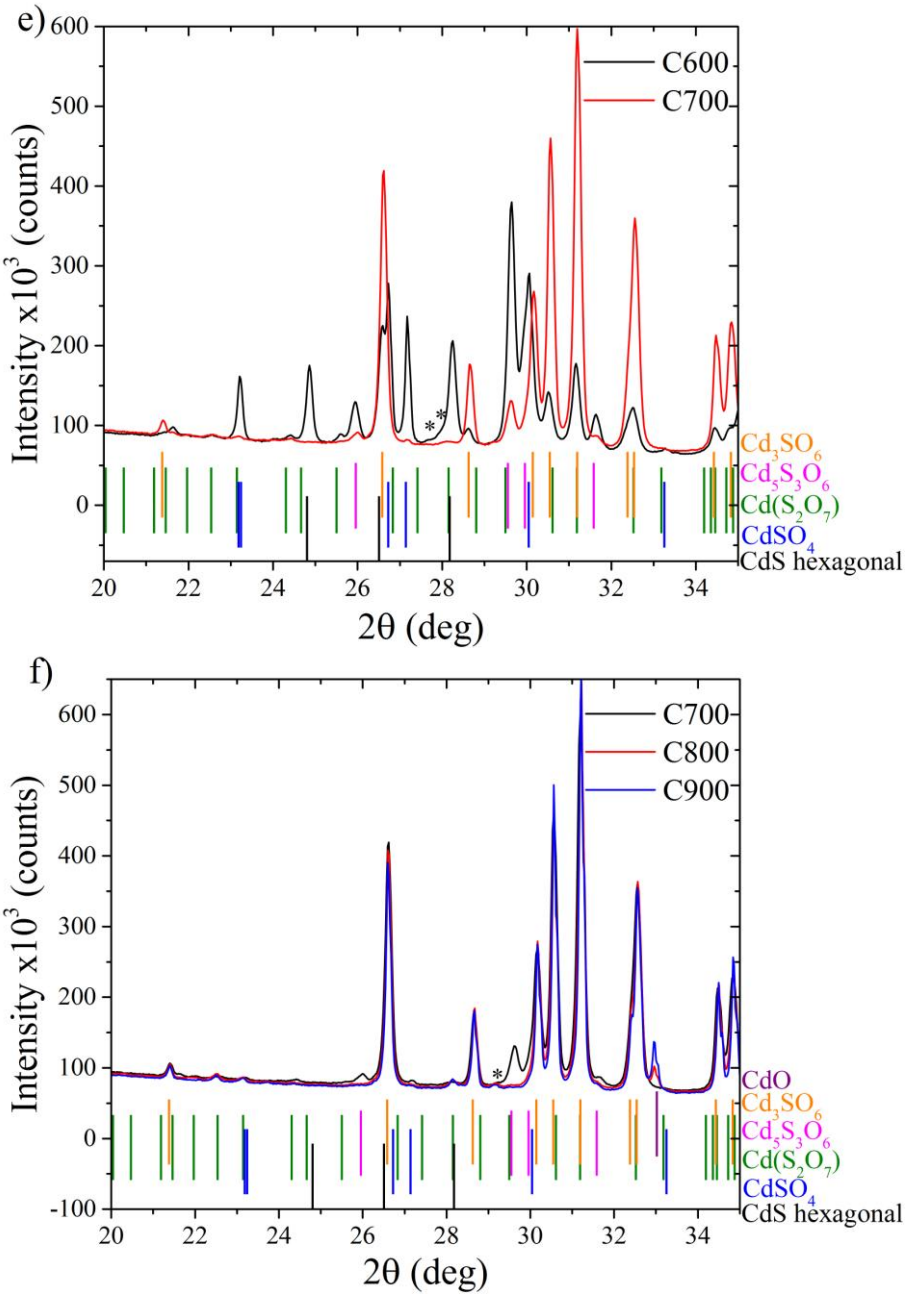

Figure S2. Evolution of X-ray diffraction patterns of CdS nanopowders annealed at different temperatures: RT-300^{o}C (a), 300-400^{o}C (b), 400-500^{o}C (c), 500-600^{o}C (d), 600-700^{o}C (e), 700-900^{o}C.

Interestingly, in the studied temperature range no reflections from $CdSO_3$ were identified. Several authors had observed the presence of cadmium sulfate(IV) at 400^{o}C[11] and between 620^{o}C and 700^{o}C[10]. However, Lee et al. had also noticed that the prolonged annealing of partially oxidized CdS leads either to the disappearance of $CdSO_3$ in an N_2

atmosphere or to the transformation into CdO in an air atmosphere[11]. The conclusion is that cadmium sulfate(IV) is unstable and easily transforms into other compounds.

Table T1. Phase composition of oxidized CdS nanopowders.

Sample	Oxidation temperature (^oC)	Phase composition						
		CdS		$CdSO_4$	$Cd(S3O_7)$	Cd_5S4O_6	Cd_3SO_6	CdO
		cubic	hex.					
RT	-	+	+	-	-	-	-	-
C100	100	+	+	-	-	-	-	-
C200	200	+	+	-	-	-	-	-
C300	300	+	+	-	-	-	-	-
C400	400	+	+	+	+	-	-	-
C500	500	-	+	+	+	+	-	-
C600	600	-	+	+	+	+	+	-
C700	700	-	(+)	+	+	+	+	-
C800	800	-	(+)	+	+	+	+	+
C900	900	-	(+)	+	+	+	+	+

3. Photocatalytic studies

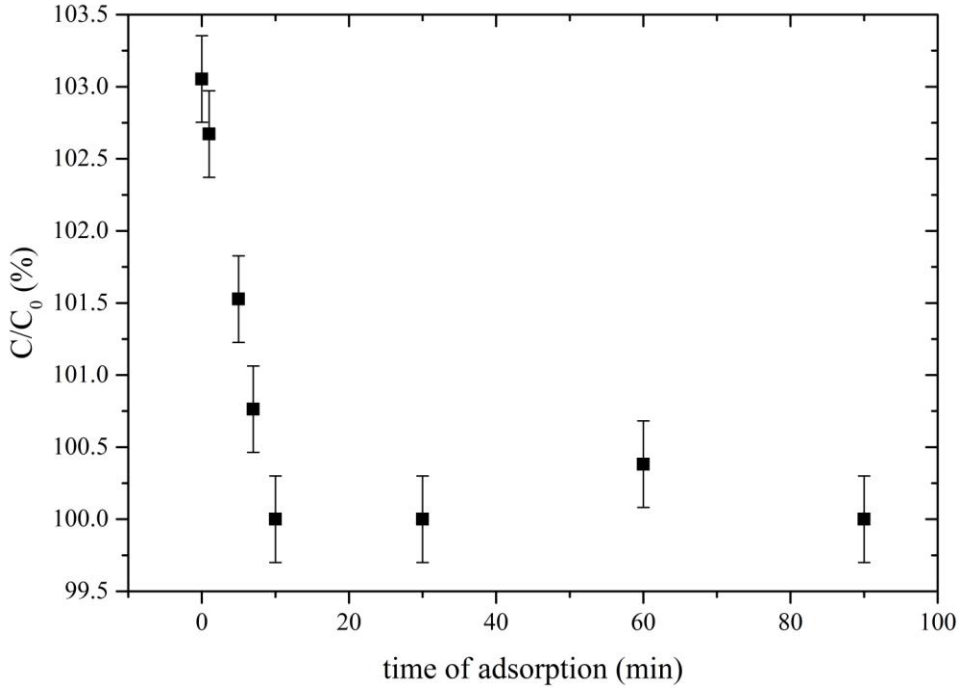

Figure S3. Example of changes of concentration of MO during the adsorption under the dark.

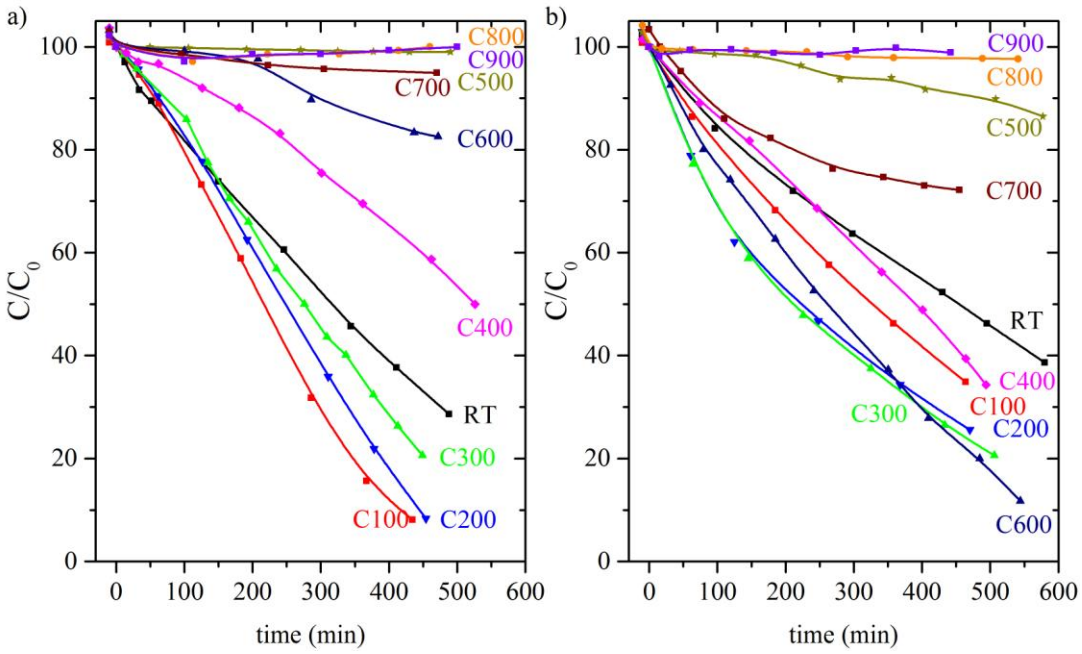

Figure S4. Degradation of MO in the presence of photocatalyst under (a) UV-vis and (b) UV light.

The Langmuir–Hinshelwood (L-H) model has been successfully used in heterogeneous photocatalysis in order to compare the photocatalytic activity of samples with regard to the mineralization of organic contaminants. L-H allows the relationship between the initial degradation rate and the concentration of the pollutant to be specified by calculating the rate of photocatalytic degradation of organic compounds. L-H can be expressed by the kinetic equation (E2):

$$r = \frac{-dC}{dt} = \frac{k_r \cdot K \cdot C}{1+(K \cdot C)} \qquad \text{(E2)}$$

Equation (E2) can easily be simplified to an apparent pseudo-first-order kinetic if the concentration of the contaminant is lower than 10^{-3} mol·dm^{-3}:

$$ln\left(\frac{C_0}{C}\right) = k \cdot K \cdot t = k_{app} \cdot t \qquad \text{(E3)}$$

where r stands for the rate of photodegradation, C represents the concentration of the reactant, t is irradiation time (s), k_r stands for the rate constant of the reaction, K is the adsorption coefficient of the reactant, and k_{app} is the apparent pseudo-first-order reaction rate constant (min^{-1}).

If the photocatalytic decomposition process is described by equation E3, the linear regression of $ln(C_0/C)=f(t)$ yields good refinement and the slope of the linear dependence is

equal to the apparent first-order rate constant (k_{app}), which can be considered to express the photocatalytic activity of the photocatalyst.

References

1 R. J. White, V. L. Budarin and J. H. Clark, *Colloids Surfaces A Physicochem. Eng. Asp.*, 2014, **444**, 69–75.

2 A. Trenczek-Zajac, J. Banaś, K. Lwierczek, K. Zazakowny and M. Radecka, *Arch. Metall. Mater.*, 2017, **62**, 841–849.

3 M. A. Simonov, S. V. Shkovror and S. I. Troyanov, *Kristallografiya*, 1988, **33**, 502–503.

4 C. Logemann and M. S. Wickleder, *Zeitschrift fur Krist. - New Cryst. Struct.*, 2013, **228**, 161–162.

5 C. Logemann and M. S. Wickleder, *Inorg. Chem.*, 2012, **50**, 11111–11116.

6 M. Pley and M. S. Wickleder, *Angew. Chemie*, 2004, **116**, 4262–4264.

7 J. Zhensheng, L. Qinglin, X. Chanjuan, J. Zhicheng and C. Zhengshi, *Appl. Surf. Sci.*, 1988, **32**, 218–232.

8 N. Fukatsu, *J. Electrochem. Soc.*, 1988, **135**, 997.

9 Y. Wei and Y. Guorui, in *Nanostructured Materials and Nanotechnology VI*, 2013, pp. 149–160.

10 S. H. Mohamed and M. El-Hagary, *Mater. Chem. Phys.*, 2013, **143**, 178–183.

11 N. Maticiuc, M. Kukk, N. Spalatu, T. Potlog, M. Krunks, V. Valdna and J. Hiie, *Energy Procedia*, 2014, **44**, 77–84.